Abdel-Malek, K. and Paul, B., (1998), "Criteria for the Design of Manipulator Arms for a High Stiffness to Weight Ratio," *SME Journal of Manufacturing Systems*, Vol. 17, No. 3, pp. 209-220.

Criteria for the Design of Manipulator Arms for a High Stiffness to Weight Ratio

Karim Abdel-Malek Department of Mechanical Engineering and
Center for Computer Aided Design, The University of Iowa, Iowa City, Iowa

Burton Paul Department of Mechanical Engineering and Applied Mechanics, University of Pennsylvania, Philadelphia, Pennsylvania.

Abstract

Design aspects of a six degree-of-freedom high accuracy manipulator are presented. The manipulator arm (called the UTI-arm) comprises four revolute and two prismatic joints. The mechanical design of the manipulator is aimed at obtaining high accuracy and a high stiffness to weight ratio of the links. Prestressing of mechanical elements is performed to transform strength to stiffness. Design of links under tension load is carried out to enhance bending stiffness. In the past, researchers have reported inefficiency of prismatic joints due to their high compliance. Compared to a uniform thin walled tube, prismatic joints used in this design provide an isotropic, higher bending stiffness, with a relatively low loss in torsional stiffness. Experiments were conducted to verify the theory presented for calculating torsional stiffness of such joints. A finite element model was also used to validate the model. The mechanical design of the arm is presented in detail in view of the proposed prismatic joint cross section and the prestressing effects.

Keywords: *Manipulator design, structural stiffness, robotics.*

Introduction

Rigid-link manipulators require light stiff structures to achieve high accuracy and low inertias. While the analysis and synthesis of revolute joints has been addressed in the literature,[1,2] prismatic joints have not had a great deal of attention due to the relative difficulty in their design and manufacture.

General handbooks to aid in the design of manipulator exist in literature.[3-6] and other works that list design criteria are also numerous.[7-11] Design of flexible mechanisms has also been addressed.[12] Analysis of stiffness of manipulator links can be found in Rivin[3] and Leu *et al*.[13]. Computer programs using computer-aided design systems[14] were employed to aid in the design of manipulator arms as early as 1979. Optimization techniques[15] and calibration techniques[16] have been used to correct errors in accuracy. Passive gravitational compensation, for example, has been addressed by Nathan and Kumar.[17]

More recently, a number of serial manipulators were designed using analytical criteria adopted for robotics technology. The UTAH/MIT arm and hand[18,19] and the WAMS system[20] are two such examples. Other robot designers have attempted to systematically develop analytical criteria for the design of critical components. For example, Feronske *et al.*[21] has set analytical criteria for the deflection prediction of serial manipulators. Henessey *et al.*[22] has demonstrated the design of a lightweight manipulator arm while Williams *et al.*[23] has demonstrated the design of an isotropic six-axis manipulator arm. Rivin[3] has compared a variety of structural material used in manipulator arms and has studied critical design components. Unique aspects of the design of manipulator arms can be found in US patents such as those by Renault,[24] Phillips,[25] and General Motors.[26] More recently, modular designs have appeared where sophisticated structures can be obtained.[27,28] Fault-tolerant methods for manipulator-joint development was introduced by Wu *et al.*[29] while the design of fault tolerant manipulators was addressed by Paredis and Khosla.[30]

In this paper, aspects of the structural design of the UTI-arm are presented. Prismatic joints of this manipulator arm are based upon a cross sectional design of the links that provides a high stiffness to weight ratio compared with a hollow round cross-section. The mechanical design of the arm will first be addressed, followed by the effect of prestressing. Stiffness of prismatic joints and comparison of experimental and theoretical results against those of tubular joints will be presented. The detailed design of the arm, controller, and interface can be found in its entirety in Abdel-Malek[31] and a related US patent.[32]

A complete detailed description of the arm will first be presented. Analytical criteria for selecting cross-sections of links used in manipulator prismatic joints will be presented. Mathematical formulations for approximating the deflection of the proposed cross-section will be derived. This cross-section will be compared with the round hollow cross-section, typically used in manipulator links. It will be shown that a significant gain in bending stiffness can be obtained with a minor loss in the torsional stiffness. Other mathematical criteria for preloading of members in tension to sustain higher bending loads will also be developed and demonstrated through comparisons with experimental results.

Description of the UTI-Arm

This section presents the UTI-arm in view of its mechanical design and assembly. Each joint will be addressed separately while the wrist joint (containing three angles) will be addressed as one entity.

Kinematic Skeleton of the UTI-Arm

Figure 1 depicts the simplified kinematic skeleton of the UTI-arm. The manipulator arm comprises six moving links (called link 1 through 6), and one stationary link (link 0). The end-effector (object holder, or gripper) is located at the end of link 6. Joint 1 is prismatic and consists of a vertical motion (d1), joint 2 is revolute θ_2, joint 3 is prismatic and consists of a horizontal motion (d3), joints 4, 5, and 6 are revolute, and are given the symbols θ_4, θ_5, *and* θ_6. The last three joints intersect at one point called the wrist point[33], which simulates a spherical wrist.

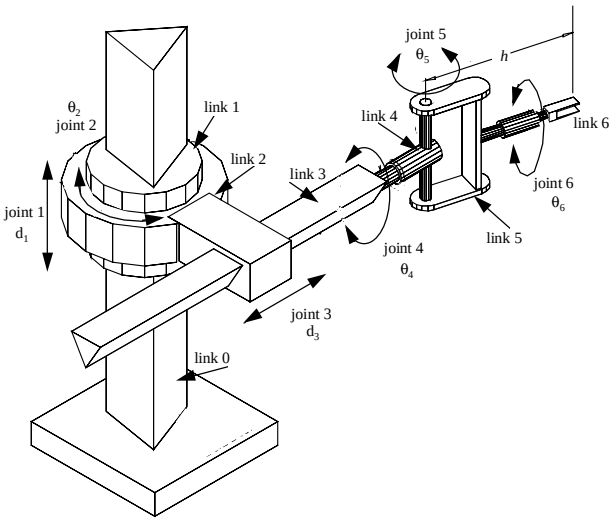

Figure 1
Kinematic Skeleton of the UTI-arm

Assembly Design

In order to simplify the forthcoming discussion, a computer rendered solid model of the arm is presented in *Figure 2*. The detailed figures used in the subsequent sections are referenced to the figure for clarity.

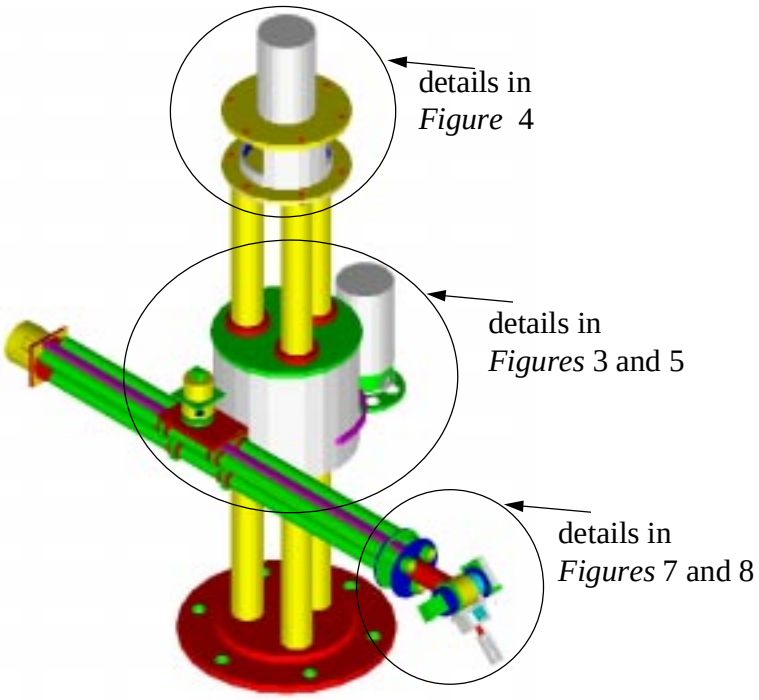

Figure 2
A computer rendered solid model of the UTI-arm

Link 0 consists of three parallel shafts fixed to a base, the centers of which are located on the vertices of an equilateral triangle. Link 1, which consists of the inner tube structure, slides vertically along link 0 using the shafts as guides thus forming Joint 1. Fastened to link 1 are six

ball-splined bushes as shown in *Figure* 3. Fastened to the bushings, are two tightening plates A and B (called thrust plates A and B in *Figure* 3). The ball splined bushings are prestressed, and the balls run inside the splined shafts. The inner tube of link 1 comprises three sections: (a) Inner tube A, (b) Ring Gear fixed to tube A, and (c) Inner tube B. An exploded view of joints 1 and 2 is depicted in *Figure* 3.

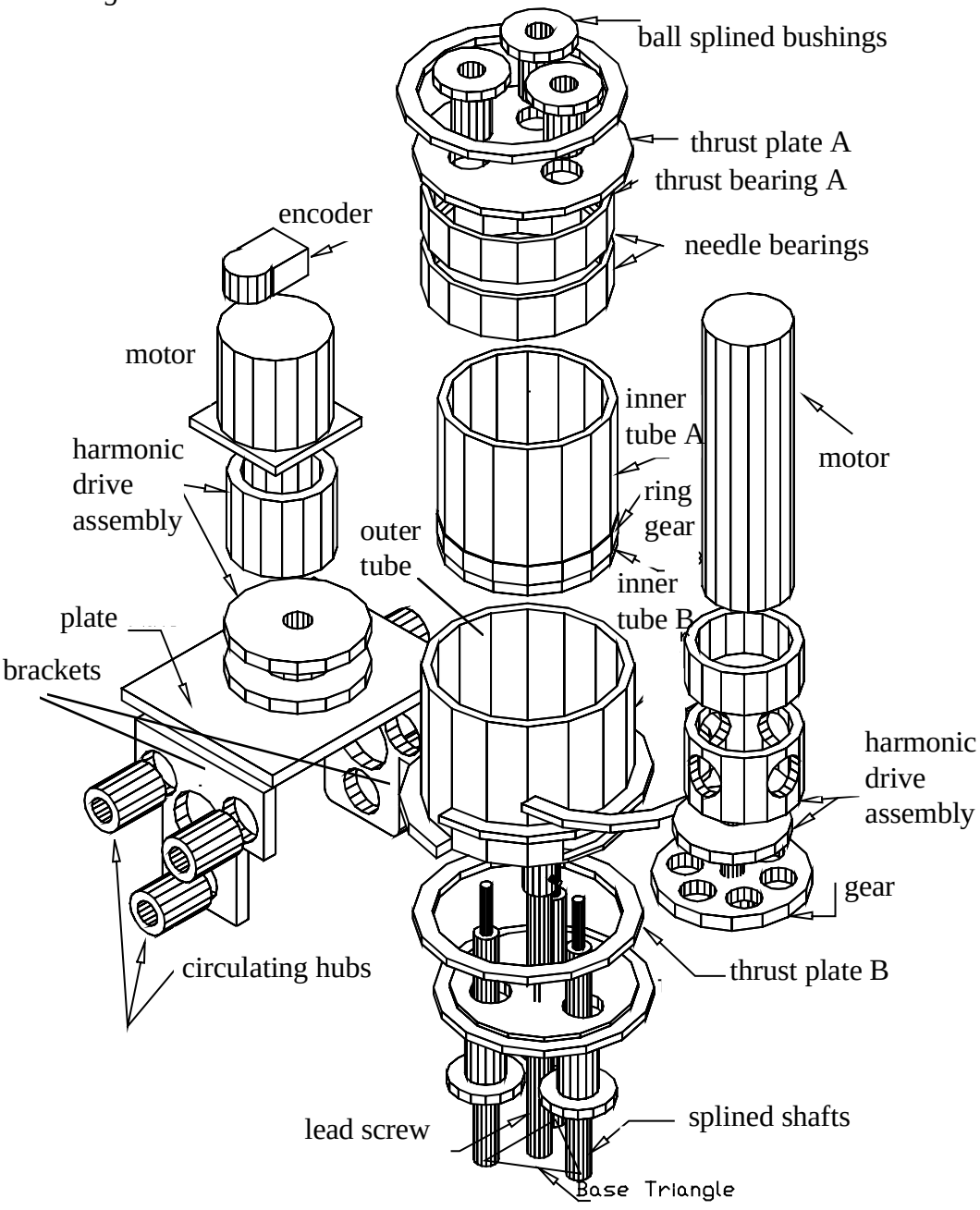

Figure 3
Exploded View of Joints 1,2, and 3

Joint 1

Joint 1, shown in *Figure 3*, is actuated via a lead screw located at the center of the base triangle (a splined shaft is located at the vertex of the triangle). A recirculating ball nut (not shown in the figure) is attached to the inner tube structure, which translates vertically along the lead screw. The lead screw is also preloaded to avoid backlash. Referring to *Figure* 4, the lead screw is directly coupled to a DC-brushless servo motor. The motor frame is fastened to the upper plate. The plate is fastened to an aluminum tubular structure (cylinder) with two flanges that are bolted respectively to the stainless steel lower and upper plates.

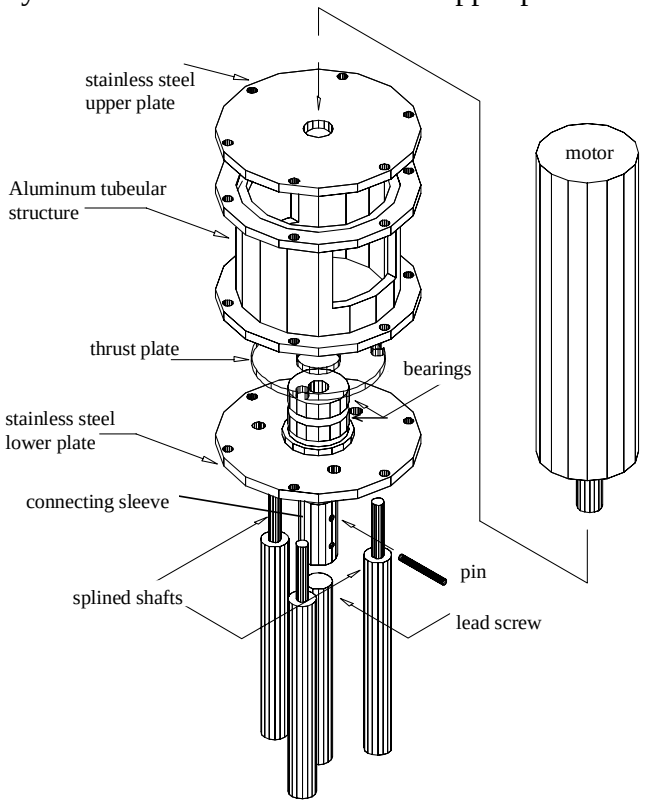

Figure 4
Exploded View of the Top Structure

Joint 2

Joint 2, shown in *Figure* 3, consists of an outer tube structure carrying the rest of the arm. The outer tube rotates around the inner tube. The weight of the outer tube is carried upon two sets of thrust bearings A and B. The plates of link 1 press the two bearings against the outer tube which allows the inner tube to carry the moment induced by the rest of the arm. The prestressing also mandates the arm to remain in position when power is shut off and eliminates the effect of clearance in the fittings. The outer tube is precisely loaded around the inner tube by the two sets of needle bearings located between the inner and outer tubes (*Figure* 3). The outer tube is rotated around the inner tube via a gear A. The gear A is allowed to rotate and translate in a circular motion (planetary gear), as sketched in *Figure* 5.

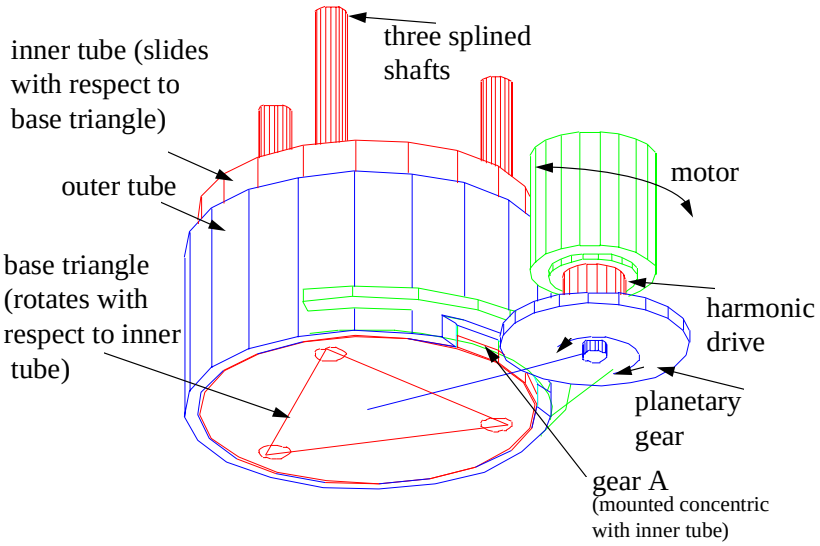

Figure 5
Gear Action

The gear is connected to a shaft that is fastened to the cup of a harmonic drive.[34] The wave generator of the harmonic drive is rotated via a DC-brushless servo motor, located coaxially with the gear and the harmonic drive. The size of the harmonic drive has been carefully chosen to take into account the pronounced compliance of the harmonic drive.

To reduce the compliance in the harmonic drive, one may either select a larger size harmonic drive, or to insert a gear immediately after the harmonic drive. Once the motor is activated, the harmonic drive transmits power to (gear A), which in turn meshes with the ring gear of link #1. The internal gear is fixed with respect to link 1 (*Figure* 5). Thus gear A is forced to rotate. However, since the structure holding gear A is fastened to the outer tube, gear A is forced to also translate.

Attached to the outer tube are two brackets (shown underneath the plate in *Figure* 3). Each bracket extends 4.5 inches from the axis of joint 1. Each bracket has three holes that are centered at the vertex of an equilateral triangle. The brackets are located at the opposite side of the motor-harmonic drive gear-assembly to compensate for weight. Connecting the two brackets is a flat plate.

Joint 3

Referring to *Figure* 6, joint 3 consists of three Inconel tubes, 20 inches long passing through a ball bushing. The tubes are located on the vertices of an equilateral triangle.

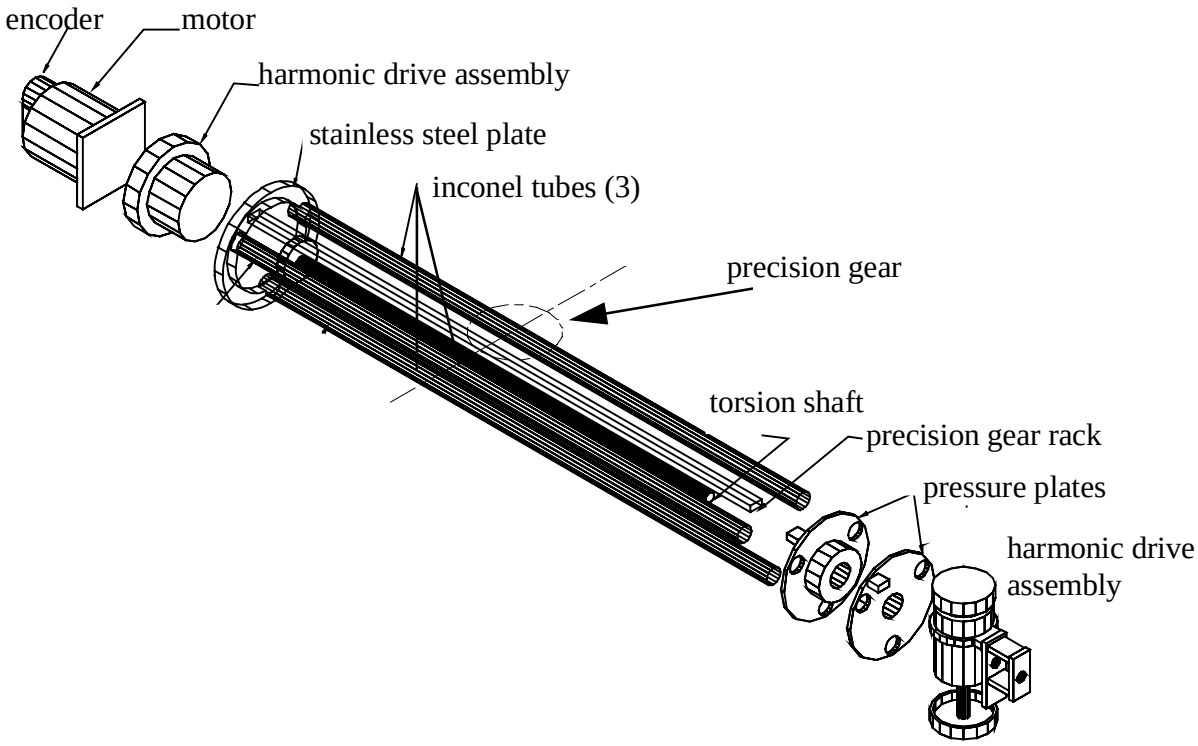

Figure 6
Joints 3 and 4 Assembly

A high precision gear rack connects the three stainless plates (one at one end holding the motor drive, and two at the other end holding the wrist). A movement of the rack will cause a movement of the three tubes as one rigid body through the brackets. The gear rack meshes with a 1 inch precision gear. The gear is fastened onto a shaft that is fastened to the cup of a harmonic drive. Connected to the harmonic drive is the actuating motor, a DC-brushless servo motor.

The wrist is located at the end of the three Inconel tubes. A shaft (shown in *Figure* 6 as the torsion shaft) attached to the wrist extends through the tubes, through the brackets and connects directly to the harmonic drive. The clamp ring of the harmonic drive is fastened to a stainless steel plate. The plate is fastened to the tubes, and the motor's frame is attached to the plate (*Figure* 6).

<u>The Wrist: Joints 4,5, and 6</u>

An exploded view of the wrist is depicted in *Figure* 7.

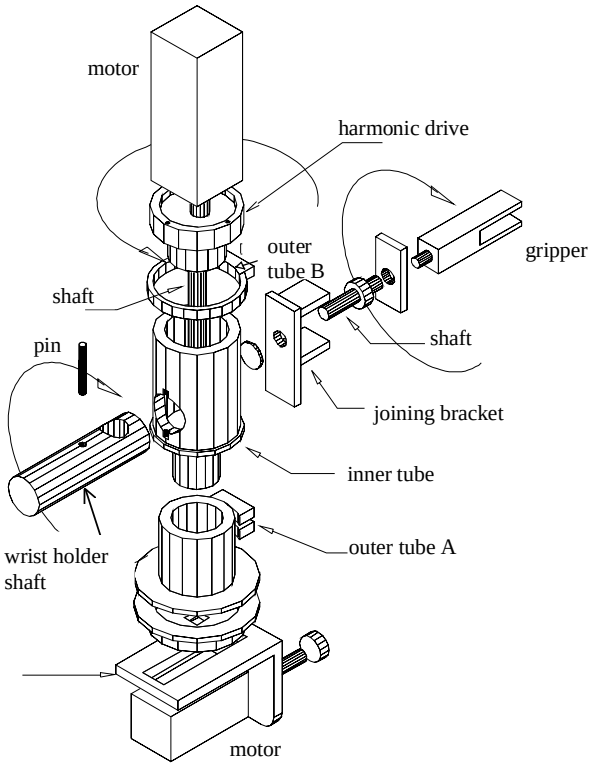

Figure 7
Exploded View of the Wrist

To position the wrist with no axial or lateral movement with respect to the tubes, two bearings are spaced by two tubular parts (see detailed design of the wrist in *Figure* 8). The shaft holding the wrist runs on these bearings. Bearings are fixed by two collars rigidly attached by six set screws.

The lateral movement is restricted by the structure of the plates having a counter bore on the inside. The bearings are separated by two hollow cylindrical spacers as depicted in *Figure* 8. The spacers are machined simultaneously to guarantee their equivalent length. The length of the inner spacer is then machined down *0.002* inches. This will insure a prestressing of the angular bearings (the outer against the inner race). The prestress would induce a considerable stiffness to eliminate clearance. The wrist rotates freely inside the two bearings, but is restricted from moving in the axial direction.

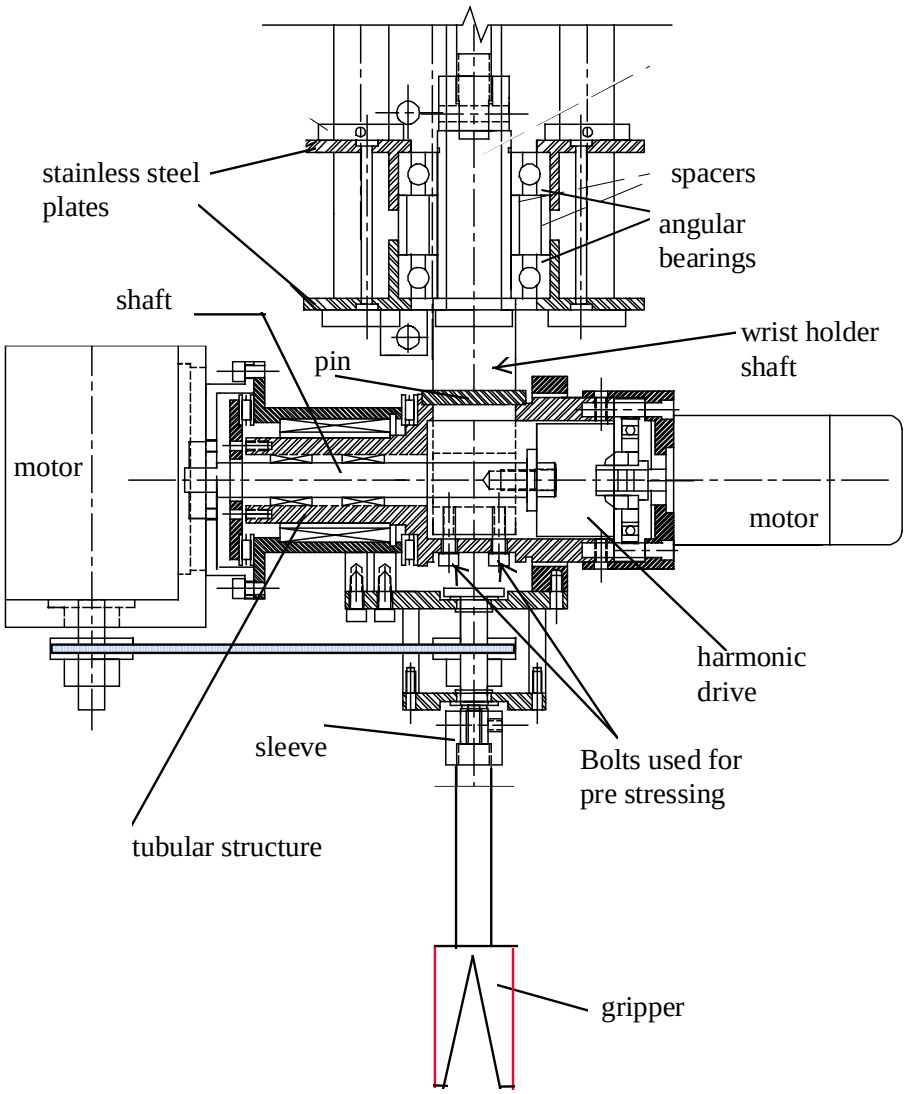

Figure 8
Details of the wrist

The wrist has a singularity when the axis of joint 4 is parallel to the axis of joint 6. The shaft of motor 5 is connected to the wave generator of a harmonic drive. The wrist structure consists of a wrist holder and a tubular structure. The wrist holder is inserted into the tubular structure at a 90^{o} angle. A pin is located through the wrist holder (the length of the pin is larger that of the diameter of the wrist holder). When fastening the wrist holder to the tubular structure, the pin is pressed against the tubular structure locking the two members into exact position and causing a state of axial tension in the wrist holder. The stress of the wrist holder shaft will transform into an enhanced bending stiffness. Higher bending stiffness allows the design of lighter distal structural links, thus lower inertia forces and higher accuracy.

The shaft through the tubular structure is connected to the cup of a harmonic drive. The clamp ring of the harmonic drive is fastened to the tubular structure. The outer tube consists of

two parts A and B (*Figure* 7), located on either side of the tubular structure. Outer tube A has a needle bearing pressed into it. The needle bearing resides on the tubular structure. The outer tube is held in position by a plate and two thrust bearings. Axial play is thereby eliminated and the stiffness in the rotational direction is enhanced.

The two parts of the outer tube A and B are connected by an aluminum structure (joining bracket in *Figure* 7). The structure consists of a U-shaped aluminum flat plates. The aluminum structure is fastened to the two parts of the outer tube. A shaft is positioned through the aluminum structure to which the end-effector may be fastened. The shaft is rotated by the motor on top of the outer tube. *Figure 9* shows the completed UTI-arm.

Figure 9
Completed UTI-arm

Preloading Effect

The design of the UTI-arm is based upon prestressing of mechanical components where possible. As shown in the above discussion, prestressing is performed in the following cases.

(a) Preloading of the ball splined bushes and shafts to enhance bending stiffness and reduce backlash.
(b) Design of the lead screw in a constant tension load to transform strength into bending stiffness
(c) Preloading of axial thrust bearings
(d) Axial preloading of angular bearings to enhance bending stiffness
(e) Design of the wrist shaft in tension to transform strength into bending stiffness
(f) Prestressing of the gear drive belt.

The following analysis demonstrates gain in bending stiffness of a link subjected to axial preloading.[35] The design of manipulator links under tension was addressed, without implementation, by Rivin,[3] but was implemented into a single link, high accuracy positioning system.[36]

To demonstrate the enhancement of stiffness due to prestressing, consider the wrist holder shaft depicted in *Figure* 8. The shaft is subjected to a bending moment as the end-effector assumes different positions. The deflection of a simply supported beam subjected to a load P and axial preload S is

$$EI\frac{d^2y}{dx^2} = Sy - \frac{l-c}{l}Px, \qquad 0 \le x < c \tag{1}$$

$$EI\frac{d^2y}{dx^2} = Sy - \frac{c}{l}P(l-x), \quad c \le x \le l \tag{2}$$

where E is the Elastic Modulus, l is the length of the cantilever, I is the second moment of area, y is the deflection, S is the axial tension force, P is the transverse load, and c is the distance from the edge to location of P. Substituting $S/EI = \kappa^2$ and solving for the left and right solutions

$$y_l = C_1\cos(i\kappa x) + C_2\sin(i\kappa x) - \frac{P(l-c)}{Sl}x \tag{3}$$

$$y_r = C_3\cos(i\kappa x) + C_4\sin(i\kappa x) - \frac{Pc}{Sl}(l-x) \tag{4}$$

where C_1, C_2, C_3, and C_4 are constants of integration. The following boundary conditions are used to find the constants

$$y_l = 0 \quad \text{for} \quad x = 0, \quad y_r = 0 \quad \text{for} \quad x = l \tag{5}$$

$$y_l(c) = y_r(l-c), \quad y_l'(c) = y_r'(l-c) \tag{6}$$

The left and right solutions can be rewritten as

$$y_l = \frac{P(l-c)}{Sl}x - \frac{P\sinh[\kappa(l-c)]}{\kappa S\sinh(\kappa l)}\sinh(\kappa x) \tag{7}$$

$$y_r = \frac{Pc}{Sl}(l-x) - \frac{P\sinh(\kappa c)}{\kappa S\sinh(\kappa l)}\sinh(\kappa(l-x)) \tag{8}$$

The maximum deflection $y_{\max}$ is observed at the middle ($x = l/2$)

$$y_{\max} = \frac{P}{2\kappa S}\left[\frac{\kappa l}{2} - \tanh\frac{\kappa l}{2}\right] \tag{9}$$

The wrist holder shaft can be approximated as a cantilever beam supported by the two bearings on one end, and loaded by the weight of the wrist and the payload on the other end. The enhanced stiffness $K_{enhanced}$ of a cantilever may be obtained by substituting 2*P* for *P* and 2*L* for *L*

$$K_{enhanced} = \frac{P}{y_{\max}} = \frac{S\kappa}{\kappa l - \tanh(\kappa l)} \tag{10}$$

While a tabulated stiffness K_s for a cantilever beam (without axial loading) is

$$K_s = \frac{P}{y_{\max}} = \frac{3EI}{l^3} \tag{11}$$

The Aluminum ($E = 10\times10^6\ psi$) wrist-holder shaft has diameter *d = 0.60"*, and a length *l = 6"*. The enhanced stiffness for a preloading of *1000 lbs* is calculated as $K_{enhanced} = 1.083\times10^3\ lbs/in$, and the stiffness without preloading is calculated as $K_s = 883.573\ lbs/in$. The ratio ($K_{enhanced}\ /\ K_s = 1.226$) indicates a 22 percent increase in stiffness. Given a yield strength σ_y and a cross sectional area *A*, the allowable axial tension (tightening the bolts shown in *Figure* 8) may achieve a maximum of $F_{allowable} = A\sigma_y$.

Prismatic Joints

Most manipulator link cross-sections are either hollow round or hollow rectangular. Hollow links provide convenient conduits for electric power and communication cables, hoses, power transmission members, etc. Rivin[3] has studied the influence of cross-sections on the deflections both in bending and torsion. He has compared hollow square with hollow circular cross sections. Rivin states that a square cross section can provide a 69 to 84 percent increase in bending stiffness over a circular hollow cross section with only a 27 percent increase in weight.

In this paper a different cross-section is introduced, consisting of three tubes centered on the vertices of an equilateral triangle. This cross section is referred to as a **tri-tube** configuration. The hollow round cylindrical link will be referred to as a **uni-tube** configuration.

Links with an open end manipulator are normally modeled as cantilevers. Consider a simple cantilever with solid or hollow cross-section with the following properties:

In pure bending, the deflection angle[37] is

$$\theta = \frac{ML}{EI} \tag{12}$$

where M is the bending moment. The tip lateral displacement is

$$\delta_{\max} = \frac{ML^2}{2EI} \tag{13}$$

In pure torsion, the twist angle is

$$\phi = \frac{TL}{GJ} = \frac{TL2(1+\nu)}{EJ} \tag{14}$$

where T is the torsional moment, G is the Modulus of Rigidity, J is the Polar moment of area, ν is Poisson's ratio, and L is the length.

The parameters that can be influenced to reduce deflections are E and *(I or J)*. The Elastic Modulus can only be changed by a change in the material. Inertias are determined mainly by the shape of the cross-section. Many studies have been performed on the choice of material for manipulator links.[3,27]

The effective length of the links may be changed by introducing a sliding support as shown in *Figure 10a*. *Figure 10b* depicts the tri-tube configuration. It may be shown that if a composite cross-section is built from any three congruent shapes located symmetrically on the sides of an equilateral triangle, the moment of inertia of the composite area about any transverse axis passing through the composite centroid is **invariant.** Therefore, the tri-tube composite section under discussion is **isotropic** in bending.

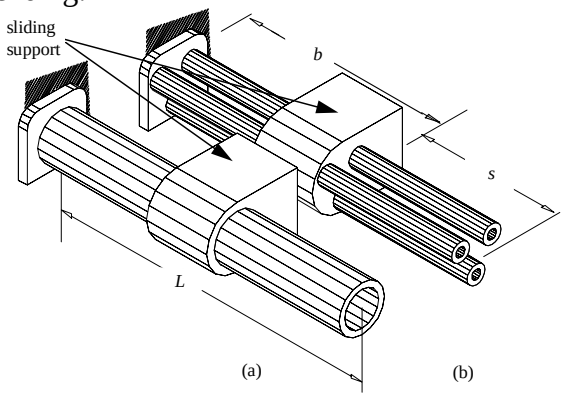

Figure 10
(a) Uni-tube Configuration (b) Tri-tube Configuration

Deflections Due to Pure Bending

To study the proposed cross-section, we utilize the following approximation for moments of inertia (2nd moment of area) about any diametrical axis through the centroid of area.

Uni-tube

For the uni-tube depicted *Figure 10a*, the moment of inertia about a diameter is

$$I_1 = \pi\frac{\left(D_0^4 - D_i^4\right)}{64} = \pi\frac{\left[D_0^4 - (D_o - 2T)^4\right]}{64} \approx \frac{\pi D_0^3 T}{8}\left(1 - 3\frac{T}{D_o} + 4\frac{T^2}{D_0^2}\right) \qquad (15)$$

where D_i and D_o are the inside and outside diameters, respectively for the uni-tube construction, T is the thickness of the uni-tube, and the area is

$$A_1 = \pi\frac{\left(D_0^2 - D_i^2\right)}{4} \approx \pi D_o T\left(1 - \frac{T}{D_o}\right) \qquad (16)$$

Tri-tube

For the tri-tube depicted in *Figure 10b*, the moment of inertia about the neutral axis *NN* is

$$I_3 = 3I_{ci} + A_i r^2 + 2A_i (r/2)^2 = \frac{3}{8}\pi t d^3\left[1 + 4\left(\frac{r}{d}\right)^2\right] \qquad (17)$$

where the moment of inertia of a single hollow tube in *Figure 11b*, about its diameter is

$$I_{ci} = \frac{\pi d_0^3 t}{8}\left(1 - 3\frac{t}{d_o} + 4\frac{t^2}{d_0^2}\right) \qquad (18)$$

and where d_o and d_i are the outside and inside diameters, respectively, for each tube on the equilateral triangle, t is the thickness of each tube in the tri-tube construction, and r *is* distance to centroid (defined in *Figure 11b).*

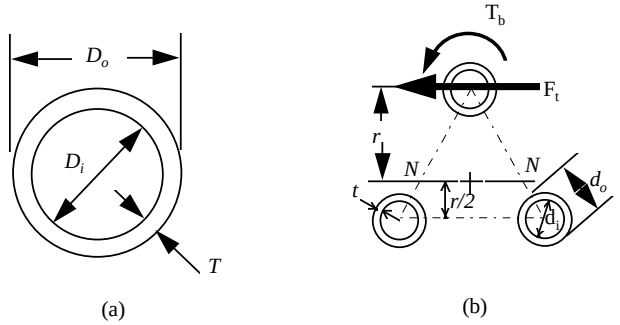

Figure 11
(a) Uni-tube Cross Section, (b) Tri-tube Cross Section

The area of each tube is

$$A_i = \pi d_o t\left(1 - \frac{t}{d_o}\right) \qquad (19)$$

From Eq. 12 and Eq. 13, and substituting *s* for *L*

$$\theta = \frac{2\delta_{\max}}{s} \tag{20}$$

Bending stiffness can be experimentally determined by using the following equation:

$$K \equiv \frac{M}{\theta} = \frac{EI}{L} = \frac{Ms}{2\delta_{\max}} \tag{21}$$

The bending stiffness for the uni-tube is

$$K_1 = \frac{EI_1}{s} \tag{22}$$

and for the tri-tube is

$$K_3 = \frac{EI_3}{s} \tag{23}$$

Angular Deflections due to Torsion

For the uni-tube cross section (*Figure 11a*), the effective length in torsion is the entire tube length *L*. For the tri-tube configuration (*Figure 11b*), the effective length in torsion is $s = L - b$, where *L* and *b* are defined in *Figure 10*. Thus ***by design***, the effective length used for calculating the twist angle has been reduced from *L* to *(L-b)*. Torsional stiffness which is proportional to $(L-b)^3$, is thereby increased considerably. The twist angle of a rod is

$$\phi = \frac{T}{K_t} \tag{24}$$

where K_t = torsional stiffness

Uni-tube

The torsional stiffness for the uni-tube construction is

$$K_1 = \frac{GJ_1}{L} \tag{25}$$

Alternately,

$$J_1 = 2I_1 \tag{26}$$

and

$$G = \frac{E}{2(1+\nu)} \tag{27}$$

Substituting Eq. 26 and Eq. 27 into Eq. 25, the stiffness can be written as

$$K_1 = \frac{E}{2(1+\nu)}\frac{2I_1}{L} \tag{28}$$

Tri-tube

The total twisting moment can be written as a combination of bending and twisting of the tubes (see *Figure 12*)

$$T = 3(F_t r + T_b) \tag{29}$$

where F_t is the tangential force acting on each tube and T_b is the Torsional moment on each tube. For the twisting moment, the twist angle is (see *Figure 12b*)

$$\phi_b = \frac{T_b}{K_b}; \quad T_b = \phi_b K_b \tag{30}$$

where the stiffness constant K_b is $$K_b = \frac{J_i G}{L} \tag{31}$$

and J_i is the polar moment of each individual tube. The twist angle ϕ_t as depicted in *Figure 12b*, is related to the tip displacement as follows

$$\phi_t = \frac{\delta_t}{r} \tag{32}$$

Where δ_t is the transverse tip displacement of each tube. At the mid section of the tube (**an inflection point in bending**), the displacement can be written as

$$\frac{\delta_t}{2} = \frac{F_t (s/2)^3}{3EI_{ci}} \tag{33}$$

Simplifying, $$\delta_t = \frac{F_t s^3}{12EI_{ci}} \tag{34}$$

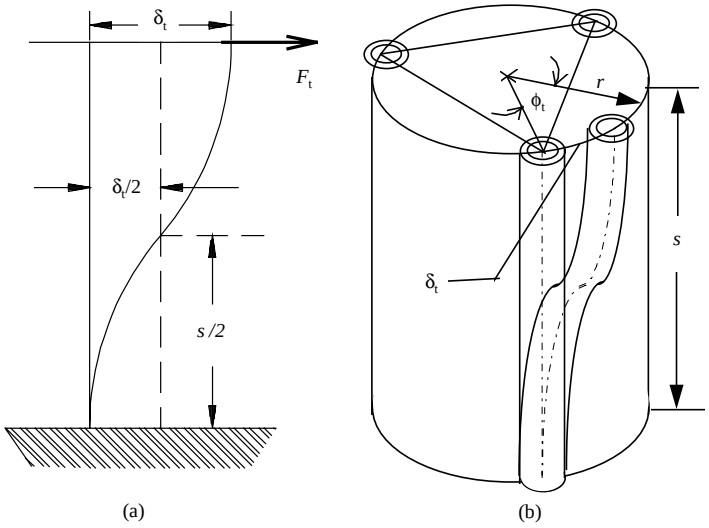

Figure 12
Torsion of the Tri-Tube Structure

Rewriting the angle as

$$\phi_t = \frac{F_t s^3}{12EI_{ci} r} \tag{35}$$

The tangential moment can now be written as

$$F_t r = \frac{12EI_{ci}\phi_t r^2}{s^3} \tag{36}$$

Substituting Eq. 36 and Eq. 30 into Eq. 29, the total twisting moment can be rewritten as

$$T = 3\left[\frac{12EI_{ci}\phi_t r^2}{s^3} + K_b\phi_b\right] \tag{37}$$

In addition, for the tri-tube configuration, the boundary condition consistent with a rigid end cap connecting all three tubes is (see *Figure 13*):

$$\phi_t = \phi_b \tag{38}$$

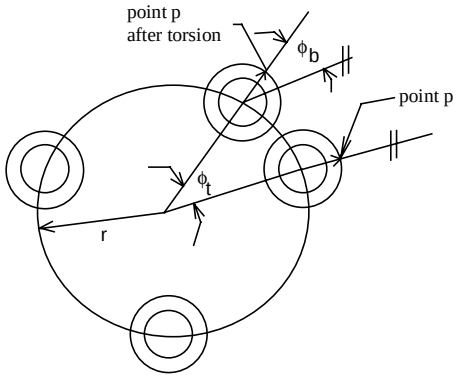

Figure 13
Boundary Conditions of a Point on the Circumference of a Tube

Upon substituting Eq. 38 and Eq. 31 into Eq. 29, we find

$$T = \left[\frac{36EI_{ci}\phi_t r^2}{s^3} + \frac{3J_{ci}G}{L}\phi_t \right] = K_3\phi_t \tag{39}$$

where K_3 is the equivalent stiffness. Substituting Eq. 26 and Eq. 27 into Eq. 39, the equivalent stiffness can be rewritten as

$$K_3 = EI_{ci}\left[36\frac{r^2}{s^3} + \frac{3}{(1+\nu)L} \right] \tag{40}$$

Comparison of Uni-Tube Versus Tri-Tube Configurations

In order to verify the theory developed in the previous section, a tri-tube configuration with the following characteristics was tested to obtain experimental results.

$d_o = 0.24"$, $d_i = 0.21"$, $I_{ci} = 6.73\times10^{-5} in^2$,

$\nu = 0.3$, $E = 27\times10^6\ psi$, $L = 13\ inch$

The tri-tube configuration was manufactured with two flanges welded at each end. High tolerances were maintained for the tube lengths and the straightness of each flange since these dimensions have a direct influence on the resulting deflection. The end of the tri-tube configuration is then held fixed while the other end is loaded and a deflection of the flange is recorded. The stiffness is calculated from the slope of the deflection-load data.

The structure was also modeled using a finite element computer program (ANSYS). Each tube is modeled as two nodes where boundary conditions for each set of end nodes are also specified. The deflection induced at one end is then plotted versus the loading at the same end. The stiffness (torsional and bending) are then calculated from the slopes of the curves. The results of torsional stiffness obtained experimentally are compared with results obtained from ANSYS and those

calculated theoretically using Eq. 40. Results are presented in Table 1. Similar results for bending stiffness are presented in Table 2.

Table 1
Torsional Stiffness

	Exp.	Theor.	FEM
Tri-tube *(r=0.6")*	311	333	309
Tri-tube *(r=1.7")*	411	409	409
Tri-tube *(r=0.6")* held at *s=3"*	324	346	331

Table 2
Bending Stiffness

	Exp.	Theor.	FEM
Tri-tube *(r=0.6")*	11134	12311	11811
Tri-tube *(r=1.7")*	105,575	95538	98641
Tri-tube *(r=0.6")*, held at *s=3"*	16035	16005	16022

For the tri-tube configuration, a significant increase in bending and torsional stiffness is noticed as the tubes are positioned further from the center of the triangle (an increase of *r* in *Figure 11b*). The increase is more significant in the case of torsion. Note the increase in stiffness as the three tubes are relocated from *r=0.6 inch* to *r=1.7 inches* (32 % increase in torsional stiffness, and 8.5% increase in bending stiffness).

By holding the *1.2 inches* tri-tube configuration at *s = 3 inches*, the increase in bending stiffness is significant (increase of 11134 to 16035 - 13%), but the increase in torsional stiffness is not as significant (increase of 311 to 324 - 4%). To compare the stiffness of the tri-tube with the uni-tube, consider a uni-tube equal in cross-sectional area (area = $0.032 in^2$), with the following properties.

$D_o = 0.489$ $D_i = 0.445$ $I_1 = 8.8 \times 10^{-4} in^4$

$\nu = 0.3$ $E = 27 \times 10^6$ *psi* $L = 13"$

The theoretical torsional and bending stiffness are presented in Table 3. For the same weight, a tri-tube configuration (with *r=1.7"*), would have 52.2 times the bending stiffness of a uni-tube. The loss in torsional stiffness, however, is not as significant (3.4%).

Table 3
Comparison of stiffness for the uni-tube and the tri-tube (theoretical)

	Torsion	Bending
Uni-tube	1406	1828
Tri-tube *(r=1.7")*	409	95538
Gain / loss in stiffness	loss in torsional stiffness **3.4%**	gain in bending stiffness **52.2%**

Equation 40 can be rewritten in dimensionless form as

$$\frac{KL}{EI_{ci}} = \left[\frac{36(r/L)^2}{(s/L)^3} + 2.3 \right] \qquad (41)$$

Figure 14 shows the influence of r and s on the torsional stiffness of the tri-tube. Note that for large values of *s*, the distance *r* has less effect on torsional stiffness, but for smaller values of s the influence of *r* becomes highly significant.

Adding a holding bracket between the two ends of the link contributes to the torsional stiffness of the tri-tube configuration. As depicted in *Figure* 3, the holding bracket has no effect on the torsional stiffness of the uni-tube configuration.

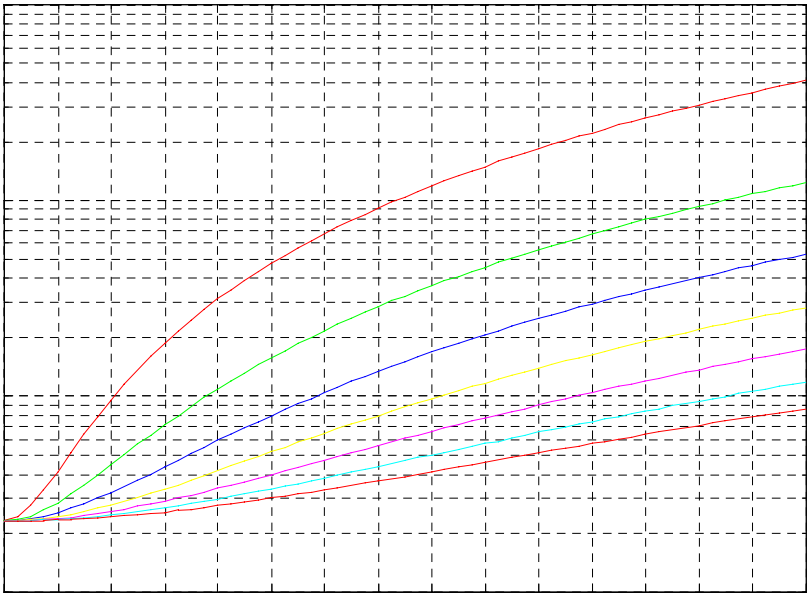

Figure 14
Semi-log plot of the effect of radius (*r*), length (*L*) and overhang (*s*) on the torsional stiffness *K*.

Conclusions

Transformation of prestressing to stiffness in manipulator links was implemented into the design of a six-axis high accuracy manipulator arm. Prestressing has shown to increase bending stiffness. Enhancement of stiffness permits the design of lighter and thus more accurate manipulator structures.

The tri-tube configuration used in the construction of prismatic joints has allowed the construction of lighter links. In comparison, the tri-tube configuration showed a higher bending stiffness than that of the uni-tube configuration, with a loss in torsional stiffness. It has also been shown that the loss of torsional stiffness is negligible compared with the gain in bending stiffness. Analytic formulation for calculating the torsional stiffness of the tri-tube configuration was validated experimentally and compared with results obtained from a finite element model. Further

comparisons need be performed between this type of prismatic joints and double revolute joints (elbow) in terms of stiffness. The analyses presented in this paper and implemented into the UTI-arm are aimed at providing a better understanding of the mechanical design of robotic arms.

Acknowledgments

This work was supported by a grant from UTI Corporation. The authors express their gratitude to Floyd Craft, Selwin Simpson, Mike Ferrel, Dave Garges, and Terri Romech for transferring ink to a working machine.

References

1. T. Kakizaki, “Modeling of Spatial Robotic Manipulators With Flexible Links and Clearance Joints,” *Transactions of the Japan Society of Mechanical Engineers*, Part C, (v57, n538, 1991), pp1961-1968.
2. E.I. Rivin, R. Holbrook, S. Bhatt, and A. Bhattacharyya, “High Stiffness/Low Inertia Revolute Link for Robotic Manipulators,” *Proceedings of the ASME Dynamics Systems and Control Division*, New York, (v6, 1987), pp253-259.
3. E.I. Rivin, *Mechanical Design of Robots*, 1988, McGraw-Hill, Inc., New York.
4. SRI International, *Robot Design Handbook*, (G. Andeen, Editor), 1988, McGraw-Hill, New York.
5. D.L. Heiserman, *How to Design and Build Your Own Custom Robot*, 1981, Blue Ridge Summit, PA.
6. S. Y. Nof, *Handbook of Industrial Robotics*, John Wiley and Sons, Inc., 1985, New York.
7. S.N. Dwivedi, "Custom Design of Robots for Specific Industrial Applications," *Design and Synthesis, Elsevier Science Publishers*, 1984, pp317-325
8. P. Minotti, and M. Dahan, "Application of Mechanisms on the Design of Robots," *Design and Synthesis, Elsevier Science Publishers*, 1984, pp347-352.
9. W.P. Seering, and V. Scheinman, Mechanical Design of an Industrial Robot, *Handbook of Industrial Robotics*, 1985, John Wiley and Sons, New York, pp44-79.
10. S. Wang, et.al., "Structure Design and Kinematics of a Robot Manipulator," *Robotica*, v6, n4, 1988, pp299-309.
11. H.J. Warneke, et al., "Mechanical Design of the Robot System," *Handbook of Industrial Robotics*, 1985, John Wiley and Sons, New York, pp80-95.
12. S. Dubowsky, and T.N. Gardner, "Design and Analysis of Multi-Link Flexible Mechanism with Multiple Clearance Connections," *ASME J. Engineering for Industry*, (v99, n1, 1977), pp88-96.
13. M.C. Leu, V. Dukovski, and K.K. Wang, “An Analytical and Experimental Study of the Stiffness of Robot Manipulators with Parallel Mechanisms,” in Donath, M., and Leu, M., (eds.), *Robotics and Manufacturing Automation, vol. PED-15, ASME*, 1985, NY, pp137-143.
14. H.J. Warneke, and R.D. Schraft, "A Computer Aided Method to Design a Manipulator," *Proc. of the 2nd Symp. on Theory and Practice of Robots and Manipulators*, 1976, Warsaw, pp101-102.
15. H. Zhuang et al., "Optimal Design of a Kinematic Accuracy Compensator for a Robot Manipulator," 1989, *IEEE Int. Conf. Rob. autom.*, vII.

16. A. Nowrozi, et. al., "Overview of Robot Calibration Techniques," *Int. Robot*, (v15, n4, 1989), pp229-232.
17. U. Nathan, and V. Kumar, "Passive Mechanical Gravity Compensation for Robot Manipulators," *IEEE Conference on Robotics and Automation*, Sacramento, CA, 1991, pp1536-1541.
18. S.C. Jacobsen, E.K. Iversen, D.F. Knutti, R.T. Johnson, and K.B. Biggers, "The UTAH/MIT Dexterous Hand: Work In Progress," *Int. J. Robotics Research*, (v3, n4, 1984) pp21-50.
19. H. Asada, K. Youcef-Toumi, and R. Ramirez, "Design of MIT Direct-Drive Arm," 1984
20. K. Salisbury, W. Townsend, B. Eberman, and D. Dipietro, "Preliminary Design of Whole Arm Manipulation System", *IEEE Conference on Robotics and Automation*, Philadelphia, PA, pp254-260.
21. D.A. Fresonke, E. Hernandez, and D. Tesar, "Deflection Predictions for Serial Manipulators," *in IEEE Conference on Robotics and Automation*. Philadelphia, PA, 1993, pp482-487.
22. M.P. Henessey, J.A. Priebe, C.H. Paul, and R.J. Grommes, "Design of a Lightweight Robotic Arm and Controller," *IEEE Conference on Robotics and Automation*, Raleigh, NC. pp779-785.
23. O.R. Williams, J. Angeles, and F. Bulca, "Design Philosophy of an Isotropic Six-Axis Serial Manipulator," *Robotics and Computer-Integrated Manufacturing*, (v10, n4, 1993) pp257-322.
24. Renault, France, "Six-Axis Manipulator," 1982, US Patent number 4348142.
25. Phillips Corp., "Manipulator Having Six Degrees Of Freedom," 1987, US Patent number 4637777.
26. General Motors Corp., "Six-Axis Manipulator," US patent number 3665148.
27. T. Fukuda, T. Veyama, Y. Kawauchi, and F. Arai, 1992, "Concept of Cellular Robotic System (CEBOT) and Basic Strategies for its Realization," *Comput. Electr. Eng*., Vol. 18, No. 1, pp. 11-39.
28. R. Hui, N. Kircanski, A. Goldenberg, C. Zhou, P. Kuzan, J. Wiercienski, D. Gershon, and P. Sinha, 1993, "Design of the Iris facility-a modular, Reconfigurable, and Expandable Robot Test Bed," *Proc. 1993 IEEE Int. Conf. Robot. Automat*., Loas Alamitos, CA, pp. 155-160.
29. E. C. Wu, J.C. Hwang, and J.T. Chladek, 1993, "Fault-Tolerant Joint Development for the Space Shuttle Remote Manipulator System: Analysis and Experiment," *IEEE Trans. Robot. Automat.*, Vol. 9, No. 5, pp. 675-684.
30. C.J. Paredis and P.K. Khosla, 1996, "Designing Fault-Tolerant Manipulators: How Many Degress of Freedom?" *Int. J. Rob. Res*., Vol. 15, No. 6, pp. 611-628.
31. K. Abdel-Malek, , *Off-Line Programming Using Commercial CAD Systems, and Design Criteria for High Accuracy Manipulators*, Ph.D. Dissertation, 1993, University of Pennsylvania, Philadelphia, PA.
32. Abdel-Malek, K., 1996, "Graphical Interface for Robot", US Patent Number 5,511,147.
33. D.L. Pieper, "The Kinematics of Manipulators Under Computer Control," Stanford Artificial Intelligence Laboratory, 1968, Stanford University, AIM 72.
34. S. Timoshenko, *Strength of Materials: Part II: Advanced Theory and Problems*, (reprint Ed.), 1976, Krieger, FL.
35. Machine Design, "Unique Positioner Improves Robot's Speed and Accuracy," Machine Design, Jan. 20, 1983, pp26-77.

36. T.J. Lardner and R.R. Archer, *Mechanics of Solids*, 1994, McGraw-Hill, New York.

Author's Biographies

Karim Abdel-Malek is an assistant professor of mechanical engineering at the University of Iowa in Iowa City. He received his MS and PhD degrees from the University of Pennsylvania in Philadelphia in mechanical engineering with emphasis in robotics. He consulted for the manufacturing industry for a number of years before joining the faculty at Iowa. He is the author of a US Patent and over thirty technical papers. His research interests are in robotics, dynamics, manufacturing, and CAD/CAM systems.

Burton Paul is ASA Whitney professor of dynamical engineering and professor of mechanical engineering at the University of Pennsylvania. He received his MS degree in engineering mechanics from Stanford University and his PhD degree from Polytechnique Institute in Brooklyn. Professor Paul was chief of the solid mechanics research group at Ingersoll Rand Research Center before joining the faculty at the University of Pennsylvania. He has been a consultant for industry in the solid mechanics, multibody kinematics and dynamics, design, robotics, and CAD/CAM systems.